http://www.jstage.jst.go.jp/browse/biophysics

BIOPHYSICS

REVIEW

Vol. 8, pp. 151–162 (2012)
doi: 10.2142/biophysics.8.151

Proposed model for the flagellar rotary motor with shear stress transmission

Toshio Mitsui[1] and Hiroyuki Ohshima[2]

[1]*Nakasuji-Yamate 3-6-24, Takarazuka, Hyogo 665-0875, Japan*
[2]*Faculty of Pharmaceutical Sciences, Tokyo University of Science, 2641, Yamazaki, Noda, Chiba 278-8510, Japan*

Received July 4, 2012; accepted September 28, 2012

Most bacteria that swim are propelled by flagellar filaments, which are driven by a rotary motor powered by proton flux. The motor consists of the rotor and the stator. The stator consists of about 8 MotA-Mot B complex. There seems to be no definite information about the structure between the rotor and the stator, and it is examined whether the experimental data can be explained based upon the following assumptions. (a) There is viscoelastic medium between the rotor and the stator. (b) MotA-MotB complex has an electric dipole moment and produces shear stress in the electric field by a proton in the channel. Calculation results based upon these assumptions are in good agreement with the following experimental observations. (1) One revolution of the flagellar rotation consists of a constant number of steps. (2) The rotation velocity of the rotor is proportional to the transmembrane potential difference. (3) When the rotational velocity of a flagellum is changed by adjusting the viscosity of the outer fluid, the torque for the cell to rotate a flagellum is practically constant but sharply decreases when the rotational velocity increases over a critical value. (4) The rotation direction remains the same when the sign of the electrochemical potential gradient is reversed. (5) The cell produces constant torque to rotate the flagellum even when the cell is rotated by externally applied torque. (6) A simple switch mechanism is proposed for chemotaxis.

Corresponding author: Toshio Mitsui, Nakasuji-yamate, 3-6-24, Takarazuka, Hyogo 665-0875, Japan.
e-mail: t-mitsui@jttk.zaq.ne.jp

Keywords: viscoelasticity,
electric field by a proton in channel,
torque-velocity relation,
irreversibility of flagellar motor,
switch mechanism for chemotaxis

Flagellar motors of most bacteria are powered by protons moving down an electrochemical gradient in channels in the membrane[1]. The motor is a complex system as illustrated, e.g., in refs. 2, 3. In the following, however, a simplified system consisting of the stator, rotor and flagellum is considered to discuss the flagellar rotation mechanism. The rotor consists of C ring, S ring and M ring (cf. Fig. 1 of ref. 2). The stator consists of MotA and MotB complexes (cf. Fig. 1 of ref. 3).

In 2000, Berg[4] summarized the constraints that any models for the flagellar rotary motor should satisfy (as summarized later in Sect. 1), and noted that none of the existing models completely satisfied the constraints. To discuss the problem, it seems worthwhile to note that the characteristics of the flagellar motor are quite different from those of F_oF_1-ATP synthase motor (for more details, cf. Appendix 1). The diameter of the flagellar motor is roughly 45 nm compared to about 10 nm of the ATP synthase motor. About 1200 protons are needed for one revolution of the flagellar motor[4], while about 10 protons can cause one revolution of the ATP synthase motor. The ATP synthase motor is reversible in the sense that reversed rotation of the rotor causes proton pumping, while there is no evidence of proton pumping for the flagellar rotor. The ATP synthase motor seems a compact, chemically specific protein machine while there seems to be no definite evidence that tight connection of protein

©2012 THE BIOPHYSICAL SOCIETY OF JAPAN

molecules exists between the rotor and stator in the flagellar motor. Around 2008, the present authors felt it worthwhile to examine whether there is any possibility that the stator can induce the rotor rotation when there is viscoelastic medium between the rotor and the stator and MotA-MotB complex has an electric dipole moment. The model proposed in the paper[5] was constructed by putting weight on the possibility. Calculation results based upon the model well explained experimental observations, satisfying Berg constraints[4]. Some readers of the paper[5], however, commented that it was very difficult to understand the model since there were many mathematical formulae whose physical meanings were only briefly explained. Also the present authors have found several immature discussions in the paper[5]. In the present review, the way of discussion in the paper[5] is largely revised and a few illustrations are added to answer the readers' comments. Also some of the mathematical symbols are altered.

Experimental data to be explained by the model are summarized in Sect. 1. Basic ideas of the model are explained in Sect. 2. The experimental data are explained by the model in Sect. 3. Summary of the study and discussion are given in Sect. 4. In Appendix 1, characteristics of the flagellar motor are compared with those of the F_oF_1-ATP synthase motor. Appendix 2 explains the way to calculate the electric field which is produced in the stator by a proton in the channel. In Appendix 3, discussion is done on the requirement on the piezoelectric property of the stator to rotate the rotor.

1. Experimental data to be explained by the model

Referring to the constraints by Berg[4], any model for the flagellar rotary motor should explain the following experimental observations.

(1) One revolution of the flagellar rotation consists of a constant number of steps irrespective of the transmembrane potential difference.
(2) The rotation velocity of the rotor is proportional to the transmembrane potential difference.
(3) When the rotational velocity of a flagellum is changed by adjusting the viscosity of the outer fluid, the torque for the cell to rotate the flagellum is practically constant independent of the velocity, but sharply decreases when the velocity increases over a critical value.
(4) There are observations that rotation direction remains the same when the sign of the electrochemical potential gradient is reversed.
(5) The cell produces constant torque to rotate the flagellum even when the cell is rotated by externally applied torque.
(6) The cell has a switch that reverses the sense of the flagellar rotation for chemotaxis.

2. The model

2.1. Basic assumptions and illustration of the model

According to Braun & Blair[6], MotA has two proton channels, and two protons practically simultaneously pass through the channels. For simplicity, however, the following discussion is done as if only one channel exists in the Mot complex and the two protons separately pass the channel. This simplification does not seem to cause any serious error in conclusion since the electric field is additive.

Discussion is done based upon the following two assumptions.

Assumption (i) MotA-MotB complex has a permanent electric dipole moment as a vector sum of dipole moments of the constituent protein molecules.
Assumption (ii) There is viscoelastic medium between the rotor and stator.

Concerning the assumption (i), it should be noted that protein molecules are structurally polar and have permanent electric dipole moments[7,8]. For instance, the dipole moment of flagellin is 800 Debye[8].

Figure 1 is an illustration of the system to be discussed with large modification of sizes and forms of the rotor constituents to make the idea of the model clear. Figure 1(a) shows the system projected on the membrane plane. The rotor is shown by the red circle. The viscoelastic medium is indicated in blue. The part of the MotA-MotB complex between the proton channel and the rotor is important in the

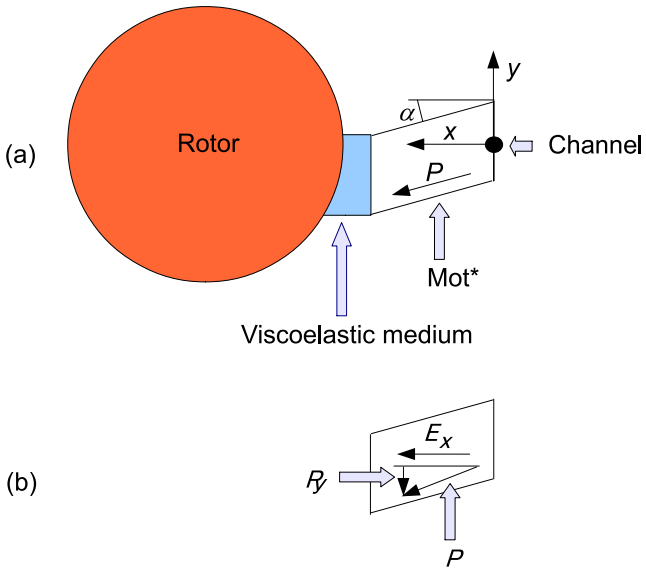

Figure 1 Schematic illustration of the system to be discussed. Sizes are not in scale. (a) A part of the flagellar rotary motor projected on the membrane plane with the coordinate system. Mot* is the part of MotA-MotB complex between the channel and the viscoelastic medium. (b) Mot* with the x component of electric field E_x and the electric dipole moment P and its y component P_y.

following discussion, and is denoted as Mot*, which is represented by the white parallelogram.

The channel is assumed to be perpendicular to the cytoplasmic membrane. The origin of the coordinate system is set at the center of the channel on the outer surface of the membrane. The z axis is set parallel to the proton channel along the proton movement and thus perpendicular to the sheet. The x axis is directed to the rotation axis of the rotor. The y axis is perpendicular to the x and z axes. The angle between the edge of the parallelogram of Mot* and the x axis is denoted as α which is a parameter to characterize the shape of Mot*. Figure 1(b) shows the inside of Mot*. E_x is the x component of electric field produced by a proton in the channel and P_y is the y component of dipole moment P.

2.2. A proton at rest in the channel

Figure 2 is to give an idea about the nature of the electric field in Mot* produced by a proton in the channel. The actual structure of Mot* is complex and calculation is done for a membrane consisting of uniform dielectric material by the method outlined in Appendix 2. The ordinate is E_x, which is the x component of electric field averaged in a volume regarded as the volume of Mot*. The abscissa is z_p/d_{ch} where z_p is the proton position on the z axis in the channel and d_{ch} is the channel length.

The order of magnitude of E_x is 10^8 V/m, which is very strong field. Note that the breakdown field strength of bulk paraffin is (0.8~1.2) × 10^7 V/m[9]. In the following we call the actual x component of the mean electric field produced by proton in Mot* as E_x for simplicity.

Suppose that the polarization P of Mot* has y component (P_y) as shown in Figure 1(b), then P tends to be parallel to E_x and a shear stress X_y appears in Mot*. The shear stress induces the strain x_y, which corresponds to the change of angle α in Figure 1(a). The shear stress X_y is proportional to the vector product of E_x and P and thus proportional to E_x and P_y and is given by

$$X_y(z_p) = aP_y(z_p)E_x(z_p) \tag{1}$$

where a is a constant.

In the present model, it is assumed that the piezoelectric activity of Mot* is the origin to cause the rotor rotation. Then a question arises how large the piezoelectric activity of Mot* should be to realize the rotor rotation. Discussion on this problem is done in Appendix 3. The conclusion there is that there is a good possibility that Mot* is designed as a shear stress transmitter to rotate the rotor.

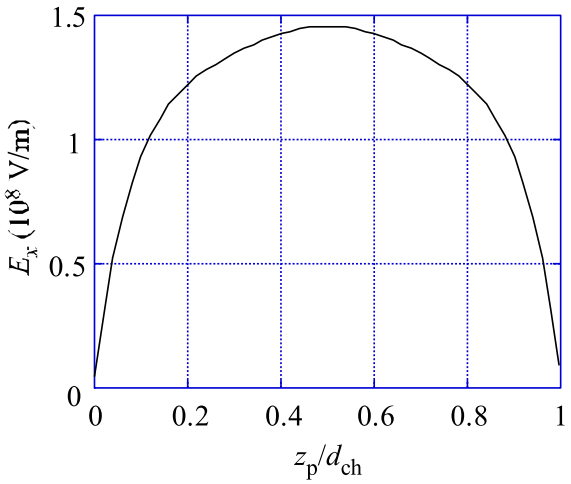

Figure 2 E_x as a function of z_p/d_{ch}. E_x: volume-averaged x component of the electric field produced in Mot* by a proton resting at z_p. d_{ch}: the channel length. Calculation is done for a simplified system and the values of E_x should be understood as approximate values. See Appendix 2 for the way of calculation.

2.3. A proton moving in the channel and shear stress flow

The transmembrane electrochemical potential $\Delta\Psi$ is defined by

$$\Delta\Psi = \Psi_{out} - \Psi_{in} \tag{2}$$

where Ψ_{out} and Ψ_{in} are the electrochemical potentials in the outer and inner liquids, respectively. It is assumed that the proton moves in the channel against constant frictional resistance, and mean velocity of all protons in channels is denoted as v_p. Then

$$v_p = A\Delta\Psi, \tag{3}$$

where A is a constant. The proton position z_p is given as a function of time t:

$$z_p = v_p t. \tag{4}$$

The field E_x produced by a proton is 0 before the proton gets into the channel and increases as the proton moves to the halfway of the channel, then decreases and becomes 0 after the proton gets out of the channel, as seen in Figure 2. During this process the energy of $e\Delta\Psi$ is liberated in Mot* and disappears in Mot*, where e is the elementary electric charge. Exact treatment of variation of E_x in such a dynamic case should be done referring to Maxwell's equations, but the proton does not seem to move very fast and the dynamics is discussed by the following approximation.

Mot* is in an elastically tensioned state with the shear stress $X_y(z_p)$ (Eq. 1) or with the associated elastic energy $U_{Xy}(z_p)$, and tends to release the tension by stress flow or energy flow out of Mot*. Parts of the flows get into the viscoelastic medium. The flows of $X_y(z_p(t))$ and $U_{Xy}(z_p(t))$ toward the rotor during dt are denoted as $J_{Xy}(t)$dt and $J_U(t)$dt, respectively, where t is time. Expressions for $X_y(z_p(t))$, $U_{Xy}(z_p(t))$, $J_{Xy}(t)$ and $J_U(t)$ are given below.

As discussed above, the stress $X_y(z_p)$ induces the strain $x_y(z_p)$. Generally, however, there is a time lag in appearing x_y. The viscoelastic medium is elastically soft and it is assumed that $J_{Xy}(t)$ flows out of Mot* within a shorter duration than the time lag of x_y and thus x_y is negligibly small. Then, in Figure 1, the angle α practically does not change during the stress flow and $P_y(z_p)$ remains almost constant at

the initial value at $E = 0$: $P_{0y}(z_p)$. Thus Eq. 1 can be approximated as

$$X_y(z_p(t)) = aP_{0y}(z_p)E_x(z_p(t)). \quad (5)$$

As usually done in the theory of elasticity, the elastic energy $U_{Xy}(z_p(t))$ is given by

$$U_{Xy}(z_p(t)) = (c_{Xy}/2)X_y(z_p(t))^2 \quad (6)$$

where c_{Xy} is an elastic constant.

The stress flow $J_{Xy}(t)$ seems to be proportional to the stress $X_y(z_p(t))$. The proportional coefficient seems to be a function of v_p and is denoted as $f(v_p)$, whose expression is determined below. Now J_{Xy}(t) is expressed by

$$J_{Xy}(t) = f(v_p)X_y(v_p t). \quad (7)$$

The energy flow $J_U(t)$ is given by

$$J_U(t) = (c_U/2)J_{Xy}(t)^2, \quad (8)$$

where c_U is an elastic constant. The total energy output from Mot* to the rotor per one proton passage is denoted as I_U:

$$I_U = \int J_U(t)\mathrm{d}t. \quad (9)$$

Here the integration is done from 0 to d_{ch}/v_p. Combining Eqs. 5 , 6, 7, 8 and 9 gives

$$I_U = \{(f(v_p)^2/v_p)(aP_{0y})^2(c_U/2)\} \int E_x(z_p)^2\mathrm{d}z_p. \quad (10)$$

Here $\int E_x(z_p)^2\mathrm{d}z_p$ is independent of v_p since $E_x(z_p)$ is the electric field component when the proton is sitting at z_p. Hence I_U depends upon v_p through the factor $f(v_p)^2/v_p$. According to Eq. 9, I_U is the integration of energy input to the rotor during one proton passage in the channel, and should be proportional to the transmembrane electrochemical potential $\Delta\Psi$, which is proportional to v_p by Eq. 3. Hence, $f(v_p)^2/v_p$ should be proportional to v_p, i.e.,

$$f(v_p) = gv_p. \quad (11)$$

Here g is a constant. Then Eq. 7 becomes

$$J_{Xy}(t) = gv_p X_y(v_p t). \quad (12)$$

By the relation $X_y(z_p) = aP_{0y}E_x(z_p)$ (Eq. 5), $J_{Xy}(t)$ becomes

$$J_{Xy}(t) = (gaP_{0y})v_p E_x(v_p t). \quad (13)$$

This expression of $J_{Xy}(t)$ is very useful. By Eq. 13, the energy flow $J_U(t) = (c_U/2)J_{Xy}(t)^2$ (Eq. 8) becomes

$$J_U(t) = \{(c_U/2)(gaP_{0y})^2\} v_p^2 E_x^2(v_p t). \quad (14)$$

Now let us consider about implication of the assumption (ii**)** that the blue part in Figure 1 is viscoelastic. The assumption implies that chemical, tight coupling by protein molecules does not exist in the blue part. However, it seems reasonable to expect that the blue part mainly consists of protein molecules. Viscoelasticity of polymers are discussed in detail in textbooks by Ferry[10] and Saito[11]. Viscoelasticity of monolayers is discussed by Langevin[12]. By the assumption (ii), the blue part behaves like an elastic body as well as like a viscous liquid. Thus shear stress flow proceeds into the viscoelastic medium due to the elasticity and viscous flow occurs in response to the shear stress due to the liquid-like property. As a simplified molecular model, let us imagine that the viscoelastic medium is an ensemble of small cylinders perpendicular to the membrane surface. The cylinders are in thermal motion in potential wells. When the shear stress exists in the medium, some cylinders change their position within wells and contribute to the elastic response of the medium. On the other hand, some cylinders move across the potential barriers by the shear stress and viscous flow takes place corresponding to the liquid-like property. After the shear stress flow passes through the medium, the elastic response within wells leaves no hysteresis, but the viscous flow over the potential barrier leaves hysteresis, causing the step motion of the rotor. Note that there is the boundary condition that material movement should be continuous at the boundaries. Accordingly, there is no slippage at the boundaries between Mot* and the viscoelastic medium and between the viscoelastic medium and the rotor. Hence the rotor rotation corresponds to the relative motion between the two boundaries.

Although the involved process is complex, we regard the shear stress flow J_{Xy}(t) = $(gaP_{0y})v_p E_x(v_p t)$ (Eq. 13) as an effective force to rotate the rotor in the following discussion. Then the parameter g is related with the nature of the viscoelastic medium.

3. Explanation of experimental observations

In this section, the subsection number and the number in parenthesis are the same as the item number of the experimental result in Sect. 1.

3.1. Experimental result (1)

(1) One revolution of the flagellar rotation consists of a constant number of steps irrespective of the transmembrane potential difference[4].

When the shear stress flow $J_{Xy}(t)$ exists at the rotor surface, the torque to rotate the rotor is $r_R J_{Xy}(t)$, where r_R is the radius of rotor. The rotation angle caused by the torque is denoted as θ. Then the friction force against the rotation is $(b\eta)\mathrm{d}\theta(t)/\mathrm{d}t$, where η is the viscosity of the outer fluid and b is a constant determined by the shape and surface condition of the flagellum. Thus we have

$$(b\eta)\mathrm{d}\theta(t)/\mathrm{d}t = r_R J_{Xy}(t). \quad (15)$$

The step rotation of the rotor due to one proton passage is indicated as $\Delta\theta$. Then, by integration of Eq. 15, we have

$$\Delta\theta = (r_R/b\eta) \int J_{Xy}(t)\mathrm{d}t, \quad (16)$$

where the integration is done from 0 to d_{ch}/v_p. If we define I_{Xy} b**y**

$$I_{Xy} = \int J_{Xy}(t)\mathrm{d}t, \quad (17)$$

$\Delta\theta$ becomes

$$\Delta\theta = (r_R/b\eta)I_{Xy}. \quad (18)$$

By the relations $J_{Xy}(t)$ (Eq. 13) and $v_p dt = dz_p$ from Eq. 4, Eq. 17 becomes

$$I_{Xy} = (gaP_{0y})\int E_x(z_p)dz_p. \quad (19)$$

Since $\int E_x(z_p)dz_p$ is the area under the curve in Figure 2, I_{Xy} is constant. Hence $\Delta\theta$ given by Eq. 18 does not depend upon $\Delta\Psi$. Accordingly, one revolution of the flagellar rotation should consist of a constant number of steps irrespective of the transmembrane electrochemical potential, as experimentally observed.

3.2. Experimental result (2)

(2) The rotation velocity of the rotor is proportional to the transmembrane potential.

The number of protons passing through one rotary motor per unit time is denoted as n. Then n is proportional to the transmembrane electrochemical potential $\Delta\Psi$. That is,

$$n = B\Delta\Psi \quad (20)$$

where B is a constant. The rotational velocity of the rotor is denoted as ω. Then ω is related with the step rotation $\Delta\theta$ by

$$\omega = n\Delta\theta. \quad (21)$$

Combining Eqs. 20 and 21 gives

$$\omega = B\Delta\Psi\Delta\theta. \quad (22)$$

Since $\Delta\theta = (r_R/b\eta)I_{Xy}$ by Eq. 18,

$$\omega = (Br_R/b\eta)I_{Xy}\Delta\Psi. \quad (23)$$

Here I_{Xy} does not depend upon $\Delta\Psi$ as proved with Eq. 19. Hence ω is proportional to $\Delta\Psi$. In Figure 3, the experimental data reported by Fung and Berg[13] are cited by black circles.

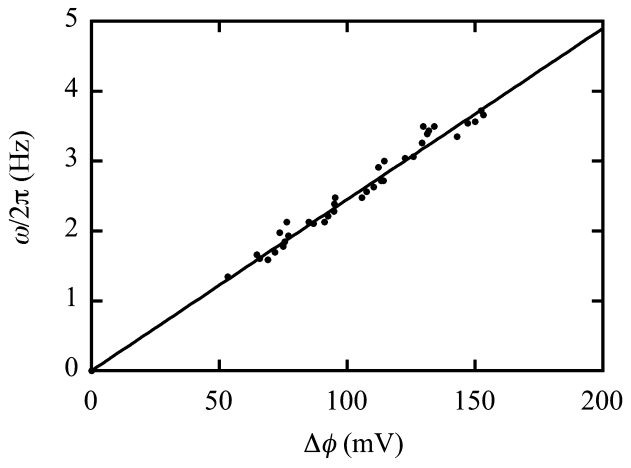

Figure 3 Flagellar rotation velocity $\omega/2\pi$ as a function of the transmembrane electric potential $\Delta\varphi$, after Figure 7 of ref. 5. The data points are cited from Figure 4 of Fuang and Berg[13].

The abscissa is the electric potential difference $\Delta\phi$ which is equal to $\Delta\Psi$ since chemical compositions in the outer and inner solutions are not changed in their study[13]. The straight line is drawn with the formula,

$$\omega/(2\pi) = 0.0245\Delta\phi \quad (24)$$

3.3. Experimental result (3)

(3) When the rotational velocity of a flagellum is changed by adjusting the viscosity of the outer fluid, the torque for the cell to rotate the flagellum is practically constant independent of the velocity, but sharply decreases when the velocity increases over a critical value.

Figure 4 shows distribution of the data points (small circles) cited from ref. 4. The abscissa is the rotational velocity $\omega/2\pi$ of the flagellum and the ordinate is the relative torque. The critical velocity is indicated as ω_{cr}. Similar data were reported for the Na^+-driven flagellar motor in Figure 4(b) of the paper by Sowa *et al.*[14], although bead sizes were changed instead of viscosity in their experiment. Change of the bead size means change of b instead of η in Eq. 15.

The following discussion is done in three parts: (1) the torque for $\omega < \omega_{cr}$, (2) the critical velocity ω_{cr}, (3) the torque for $\omega > \omega_{cr}$

3.3.1. The torque for $\omega < \omega_{cr}$

The torque to rotate the rotor is denoted as T. The observed torque is obtained by multiplying the viscous resistance $b\eta$ and the rotation velocity ω:

$$T = b\eta\omega. \quad (25)$$

By $\Delta\theta = (r_R/b\eta)I_{Xy}$ (Eq. 18) and $\omega = B\Delta\Psi\Delta\theta$ (Eq. 22), we have

$$T = Br_R\Delta\Psi I_{Xy}. \quad (26)$$

Note that the viscosity-dependent term $b\eta$ disappears in Eq. 26. Since I_{Xy} is a constant as proved with Eq. 19, the torque T remains constant irrespective of the viscosity η for given $\Delta\Psi$. In Figure 4, the horizontal line (ω) indicates the relative value of torque $T(\omega)/T(\omega_{cr})$, which is constant according to this conclusion. The experimental data are distributed around the straight line (ω) for $\omega < \omega_{cr}$.

3.3.2. The critical velocity ω_{cr}

The rotation of the flagellum in the viscous solution causes energy dissipation. Let the energy liberation during dt be $D_\eta dt$ in the step rotation $\Delta\theta$. Then D_η is given by the frictional torque $b\eta d\theta/dt$ multiplied by the rotation velocity $d\theta/dt$:

$$D_\eta(t) = b\eta(d\theta/dt)^2. \quad (27)$$

Since $(b\eta)d\theta(t)/dt = r_R J_{Xy}(t)$ (Eq. 15) at the stationary rotation, $D_\eta(t)$ becomes

$$D_\eta(t) = r_R^2 J_{Xy}(t)^2/(b\eta). \quad (28)$$

Since $J_{Xy}(t)$ is independent of η, Eq. 28 implies that the

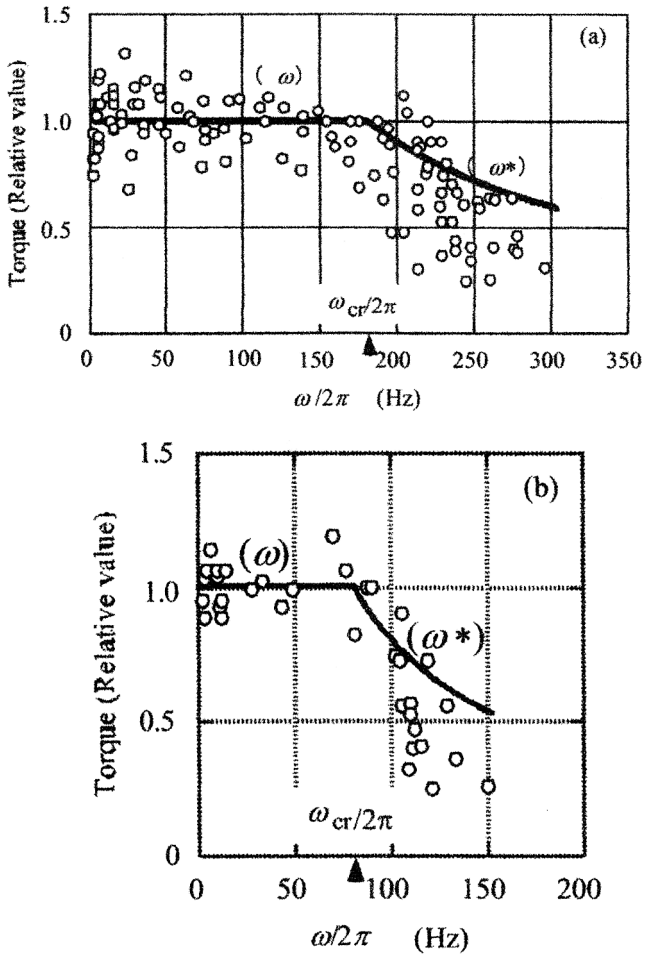

Figure 4 Relative value of torque as a function of the rotation velocity $\omega/2\pi$, after Figure 8 of ref. 5. Data points (small circles) are cited from Figure 3 of Berg[4]. (a) 23°C and (b) 16°C. The horizontal line (ω) represents the relative torque according to the conclusion by Eq. 26 that the torque is constant for $\omega < \omega_{cr}$. The curve (ω^*) is the relative torque ω_{cr}/ω (Eq. 44), which gives the upper limit of the relative torque for $\omega > \omega_{cr}$.

energy dissipation $D_\eta(t)$ becomes infinitely large as η approaches to 0. This is impossible and the necessary condition for the stationary flagellar rotation is given by

$$D_\eta(t) < J_U(t) \tag{29}$$

where $J_U(t)$ is the energy input during dt and given by $J_U(t) = (c_U/2)J_{Xy}(t)^2$ (Eq. 8). Combining Eqs. 8, 28 and inequality in Eq. 29 gives

$$\eta > 2r_R^2/(bc_U). \tag{30}$$

Now η_{cr} is defined by

$$\eta_{cr} = 2r_R^2/(bc_U). \tag{31}$$

Then the condition for the stationary rotation of the flagellum is given by

$$\eta > \eta_{cr}, \tag{32}$$

In the stationary rotation, ω is given by $\omega = (Br_R/b\eta)I_{Xy}\Delta\Psi$ (Eq. 23). Hence the critical velocity ω_{cr} corresponding to η_{cr} is given by

$$\omega_{cr} = (Br_R/b)I_{Xy}\Delta\Psi/\eta_{cr}. \tag{33}$$

Or by Eq. 31,

$$\omega_{cr} = \{Bc_U/(2r_R)\}I_{Xy}\Delta\Psi. \tag{34}$$

The range of constant torque is limited in the range

$$\omega < \omega_{cr}. \tag{35}$$

Accordingly, the straight line (ω) is terminated at ω_{cr} in Figure 4.

3.3.3. The torque for $\omega > \omega_{cr}$

When $\eta < \eta_{cr}$, all the input energy flow $J_U(t)$ will be absorbed by the flagellar rotation, although there is no balance of forces expressed by $(b\eta)\mathrm{d}\theta(t)/\mathrm{d}t = r_R J_{Xy}(t)$ (Eq. 15). Presumably the flagellum rotates at random, but here let us suppose a fictional case that the rotation is smooth with a rotation velocity θ^*. Then the energy liberation rate is given by multiplication of the torque $b\eta\mathrm{d}\theta^*/\mathrm{d}t$ and the rotation velocity $\mathrm{d}\theta^*/\mathrm{d}t$. If this energy dissipation rate is set equal to the energy input $J_U(t)$ given by $J_U(t) = (c_U/2)J_{Xy}(t)^2$ (Eq. 8), we have

$$b\eta(\mathrm{d}\theta^*/\mathrm{d}t)^2 = (c_U/2)J_{Xy}(t)^2. \tag{36}$$

Thus

$$\mathrm{d}\theta^*/\mathrm{d}t = J_{Xy}(t)\{c_U/(2b\eta)\}^{1/2}. \tag{37}$$

By using I_{Xy} in Eq. 17, integration of Eq. 37 gives

$$\Delta\theta^* = I_{Xy}\{c_U/(2b\eta)\}^{1/2}. \tag{38}$$

The corresponding rotation velocity ω^* is given by

$$\omega^* = n\Delta\theta^* = nI_{Xy}\{c_U/(2b\eta)\}^{1/2}. \tag{39}$$

The parameters other than η are independent of η. If the parameters other than η are combined and expressed by a constant C^*, then

$$\omega^* = C^*/\eta^{1/2}. \tag{40}$$

The torque T^* is defined by $b\eta\omega^*$. Then

$$T^* = bC^*\eta^{1/2}. \tag{41}$$

Combining Eqs. 40 and 41 gives

$$T^* = bC^{*2}/\omega^*. \tag{42}$$

Hence we have

$$T^*(\omega^*)/T^*(\omega_{cr}) = \omega_{cr}/\omega^*. \tag{43}$$

To see the nature of Eq. 43, ω^* is replaced by ω as

$$T^*(\omega)/T^*(\omega_{cr}) = \omega_{cr}/\omega \tag{44}$$

This relation is plotted as the curves (ω^*) in Figure 4(a) and (b). The curve $T^*(\omega)/T^*(\omega_{cr}) = \omega_{cr}/\omega$ is continuous with

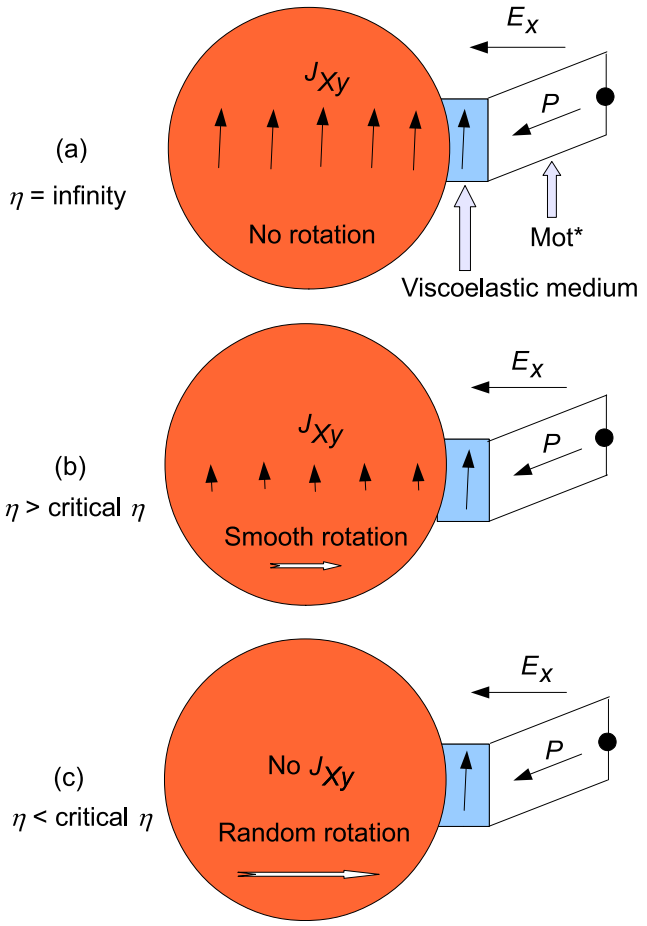

Figure 5 Transmission of the shear stress flow J_{Xy}. (a) The viscosity η of the outer liquid is infinitely large. The rotor does not rotate and all J_{Xy} transmits into the inside of the rotor. (b) η has a finite value larger than η_{cr}. The rotor smoothly rotates by using a portion of the input energy. The remaining part transmits into the inside of the rotor. (c) η is smaller than η_{cr}. All input energy is used for random rotation of the rotor.

$T(\omega)/T(\omega_{cr}) = 1$ at $\omega = \omega_{cr}$. The flagellar rotation seems to be random for $\omega > \omega_{cr}$ and the data points are expected to distribute under the curve (ω*) which is derived on the assumption of fictional smooth rotation. In the calculation, the parameter values of ω_{cr} are determined based upon this expectation.

Curve (ω*) more steeply declines in Figure 4(b) than in (a). The distribution of data points shows similar tendency.

Figure 4(a) for 23°C and (b) for 16°C indicate that ω_{cr} sensitively depends upon temperature. It is a possibility that the viscoelastic medium becomes less liquid-like at lower temperature and reduces the shear stress input to the rotor (I_{Xy}), and causes a decrease of ω_{cr} which is given by $\omega_{cr} = \{Bc_U/(2r_R)\}I_{Xy}\Delta\Psi$ (Eq. 34).

Figure 5 is to help understanding the discussion in this section. Figure 5(a) shows the case that the viscosity of the outer fluid η is infinitely large. The rotor does not rotate and all the shear stress flow J_{Xy} propagates into the inside of the rotor without loss. In (b) η has a finite value larger than η_{cr}. The rotor rotation takes place with the force balance expressed by $(b\eta)\mathrm{d}\theta(t)/\mathrm{d}t = r_R J_{Xy}(t)$ (Eq. 15) using a portion of J_{Xy}. The remaining part of J_{Xy} proceeds into the inside of the rotor. In (c) $\eta < \eta_{cr}$, and all $J_{Xy}(t)$ is used for random rotation of the rotor.

Let us consider about the energy efficiency of the flagellar motor, e_U Since the energy dissipation rate in the rotor rotation is given by $D_\eta(t) = r_R^2 J_{Xy}(t)^2/(b\eta)$ (Eq. 28) and all the energy dissipation per one proton passage is given by $(e\Delta\Psi)$, the energy efficiency e_U is given by

$$e_U = k\int D_\eta(t)\mathrm{d}t/(e\Delta\Psi) = kr_R^2\int J_{Xy}(t)^2\mathrm{d}t/(e\Delta\Psi b\eta). \quad (45)$$

Here k is a constant. In this equation, parameters other than η do not depend upon η, and hence we have

$$e_U(\eta)/e_U(\eta_{cr}) = \eta_{cr}/\eta, \text{ for } \eta > \eta_{cr}. \quad (46)$$

By Eq. 23, Eq. 46 becomes

$$e_U(\omega)/e_U(\omega_{cr}) = \omega/\omega_{cr}, \text{ for } \omega < \omega_{cr}. \quad (47)$$

Thus the efficiency e_U increases with increasing ω for $\omega < \omega_{cr}$, and then decreases with increasing ω since randomness in the rotation reduces e_U for $\omega < \omega_{cr}$.

3.4. Effect of reversal of the sign of the electrochemical potential gradient

(4) There are observations that the rotation direction remains the same when the sign of the electrochemical potential gradient is reversed.

In 1980, Manson, *et al.*[15] used *Streptococcus* bacteria and examined how the flagellar rotation velocity varies when the sign of the transmembrane electrochemical potential is reversed by changing ionic concentration in the outer solution. They observed that in some specimens, the direction of the rotation remained the same but in other specimens the direction was reversed when the proton movement was reversed. In 1982, Berg *et al.*[16] carried out more detailed studies of the effects. They examined how the rotation velocity changes when pH changes from 7 to 8 in the outer solution. The rotation velocity became 0 around pH = 7.5. Experimental results were not very reproducible when pH was changed in the outer solution but there were cases that the rotation occurred in the same direction in both sides of pH = 7.5. An example of their results is cited by black circles in Figure 6. As pH increases from pH = 7.0, velocity ω decreases, becomes 0 around pH = 7.5, and then increases. The direction of the proton passage seems to be reversed at pH = 7.5, but the rotation takes place in the same direction in both sides of pH = 7.5.

Our model supports the experimental results in Figure 6 as discussed below. Hitherto we have discussed the case that the electrochemical potential Ψ_{out} of the outer solution is higher than Ψ_{in} of the inner potential. The transmembrane electrochemical potential is defined by $\Delta\Psi = \Psi_{out} - \Psi_{in}$ (Eq. 2) and the proton velocity v_p is expressed by $v_p = A\Delta\Psi$

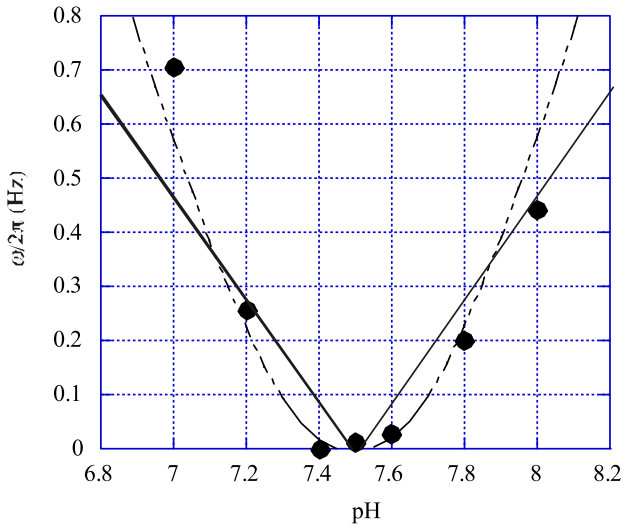

Figure 6 Flagellar rotation velocity $\omega/2\pi$ as a function of pH of the outer solution, after Figure 9 of ref. 5. Data points are cited from Fig. 5b of Berg *et al.*[16]. The direction of the proton is inward for pH < 7.5 and outward for pH > 7.5, but the direction of the rotation remains the same in both sides of pH = 7.5.

(Eq. 3). To discuss the case that $\Delta\Psi$ changes its sign at pH = 7.5, we define v_p by

$$v_p = A|\Delta\Psi|. \tag{48}$$

The proton positions in the channel $z_p(t)$ are given by $z_p(t) = v_p t$ when $\Psi_{out} > \Psi_{in}$, while $z_p(t) = d_{ch} - v_p t$ when $\Psi_{out} < \Psi_{in}$. In both cases, the electric field $E_x(t)$ is produced by the proton as shown in Figure 2: $E_x(t)$ is 0 at $t = 0$, becomes maximum around $t = d_{ch}/(2v_p)$ and returns to 0 at $t = d_{ch}/v_p$. Thus the change of $E_x(t)$ is similar although the direction of proton motion is reversed. Accordingly, we can use $J_{Xy}(t) = (gaP_{0y})v_p E_x(z_p(t))$ (Eq. 13) and $J_U(t) = \{(c_U/2)(gaP_{0y})^2\}v_p^2 Ex^2(z_p(t))$ (Eq. 14) in both cases of $\Psi_{out} > \Psi_{in}$, and $\Psi_{out} < \Psi_{in}$. As a result, the rotor rotates in the same direction with the same velocity irrespective of the sign of $\Delta\Psi$ in accordance with the experimental results shown in Figure 6.

The rotation velocity ω is proportional to the potential difference $|\Delta\Psi|$ when $|\Delta\Psi|$ is relatively large as shown in Figure 3. If this relation holds for small $|\Delta\Psi|$, the ω vs. pH relation becomes as shown by the straight lines in Figure 6. The experimental data, however, indicate the tendency that tangent of the ω vs. pH relation becomes 0 in the vicinity of pH = 7.5, as indicated by the quadratic curve. The values of ω plotted in Figure 6 are smaller than those in Figure 3, and hence proton velocities should be smaller in the case of Figure 6. Therefore, the results in Figure 6 mean that slowly moving proton does not effectively produce the shear stress flow. Two causes can be considered to explain it. In deriving Eqs. 5 and 7, it is assumed that the shear stress flow $J_{Xy}(t)$ occurs within a shorter duration than the time lag of x_y and x_y is negligibly small. It is, however, plausible that x_y becomes large so that effectiveness of $J_{Xy}(t)$ is reduced when the proton moves very slowly. Also, the viscoelastic medium generally loses its ability to transmit the shear stress when the shear stress slowly changes.

3.5. Experimental result (5)

(5) The cell produces constant torque to rotate the flagellum even when the cell is rotated by externally applied torque.

Berg and his colleagues[16–18] used the technique of electrorotation to apply the torque to cells of bacteria tethered to glass coverslips by a single flagellum. Cells were driven to rotate either forward or backward. Here forward means the direction of rotation driven by the flagellar motor itself. They used the intact cells which could normally rotate the flagellum (called motor intact) and the broken cells which lost the ability to rotate the flagellum (called motor broken). Berg and Turner[17] observed a barrier to backward rotation for the motor intact but later Berry and Berg[18,19] found that it was an artifact. According to Berry and Berg[18,19], the relation between the rotation velocity of motor intact and the torque is approximately linear from −100 Hz to +100 Hz and parallel to the relation of motor broken.

To make the experimental results clear, let us denote the externally applied torque as T_{app} and the rotation velocities of the broken and intact cells as $\omega_{brk}(T_{app})$ and $\omega_{int}(T_{app})$, respectively. Then the experimental results by Berry and Berg[18,19] are expressed by the two formulae.

$$\omega_{brk}(T_{app}) = qT_{app}, \tag{49}$$

$$\omega_{int}(T_{app}) = qT_{app} + \omega_{int}(0). \tag{50}$$

Here q is a constant and $\omega_{int}(0)$ is the rotation velocity produced by the intact cell in the absence of T_{app}. Figure 7 shows lines ω_{int} and ω_{brk} corresponding to Eqs. 49 and 50.

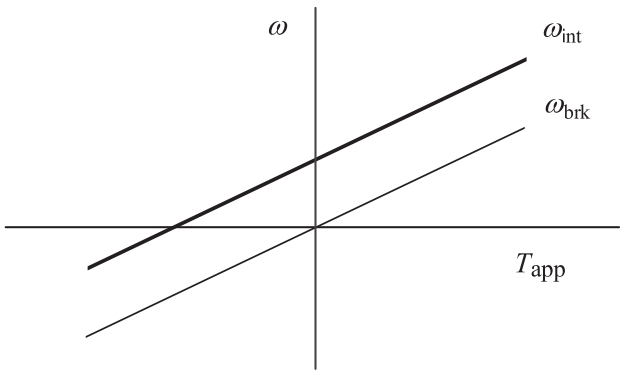

Figure 7 Illustration of the effect of the externally applied torque on the flagellar rotation velocity, after Figure 10 of ref. 5. The cell is tethered by a single flagellum and the cell body is rotated electrically[18,19]. T_{app}: externally applied torque on the cell. ω_{int}: measured rotation velocity of the intact cell when the torque is applied externally. ω_{brk}: measured rotation velocity of the broken cell when the torque is applied externally.

As mentioned above, Berg and his colleagues[17–19] used the technique of electrorotation to apply the torque to cells tethered to glass coverslips by a single flagellum. Theoretically, the relative motion between the cell and a flagellum is important, and the following discussion is done as if the cell is fixed and a flagellum is rotated by an external torque. The externally applied torque T_{app} to the flagellum rotates the rotor. Then the rotor produces shear stress in the viscoelastic medium and in Mot*. Mot* deformed and an electric field is induced by piezoelectricity in Mot*. The transmembrane elecrochemical potential $\Delta\Psi$ is, however, kept constant by the outer and inner liquids and the variation of the electric field inside of Mot* should satisfy this boundary condition. Accordingly, the mean electric field in the channel due to $\Delta\Psi$ remains constant and the cell produces almost the same torque as in the absence of externally applied torque, resulting in the relation $\omega_{int}(T_{app}) = qT_{app} + \omega_{int}(0)$ (Eq. 50). Naturally the reversed rotation of the rotor does not induce proton pumping.

3.6. Experimental observation (6)

(6) The cell has a switch which reverses the sense of the flagellar rotation for chemotaxis.

One possible mechanism for the switch is that Mot* has two stable structures having positive and negative P_{0y} as illustrated in Figure 8. Information flow from the receptor to the flagellar motor in the chemotaxis is illustrated, e.g., in Figure 2 of ref. 20. If there is a device to interchange the two structures in Figure 8 simultaneously in all Mot*s in response to the information flow, the shear forces $J_{Xy}(t) = (gaP_{0y})v_pE_x(v_pt)$ (Eq. 13) change their signs in all Mot*s and the direction of flagellar rotation is reversed for the chemotaxis. Presumably the proposed mechanism is simpler than in the case of chemically tight coupling models.

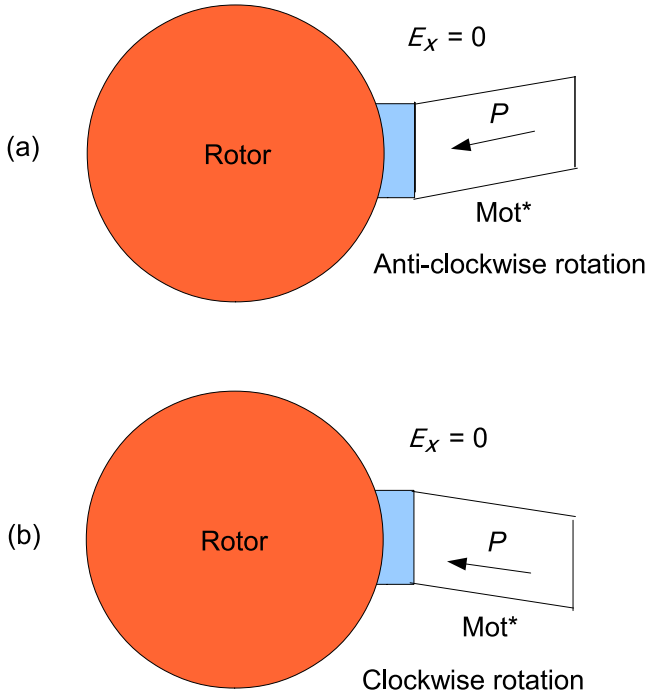

Figure 8 Proposed mechanism for reversal of the rotation direction in the chemotaxis. (a) The dipole moment P has the downward component and causes anti-clockwise rotor rotation. (b) The dipole moment P has the upward component and causes clockwise rotor rotation.

4. Summary and discussion

The study described above started from the question of whether there is any possibility that the stator can induce the rotor rotation in the absence of chemically tight connection by protein molecules between them. We assume that there is only viscoelastic medium between the rotor and stator and that Mot* has a permanent electric dipole moment. Then Mot* acts as a shear stress generator through the interaction between its dipole moment and the electric field produced by a proton passing in the channel. The shear stress transmits through the viscoelastic medium and leaves hysteresis which causes the step rotation of the rotor. Calculation results based upon the model well explain experimental observations as described in Sect. 3, and suggest that the proposed model is not very far from reality. For further discussion, however, detailed experimental data are needed on the nature of the viscoelastic medium and electric and piezoelectric properties of the Mot assembly.

One of the characteristic features of our model is that discussion is done on the basis of the force balance expressed by $(b\eta)\mathrm{d}\theta(t)/\mathrm{d}t = r_R J_{Xy}(t)$ (Eq. 15) instead of the energy balance. Related shear stress flow is illustrated in Figure 5.

As noted in our previous review on muscle contraction mechanism[21], protein molecules are structurally polar and biological systems should be considered as a system of four variables (electric field, polarization, stress, and strain) from the physical view point. The present study is based upon this idea. Systematic discussion on four variable systems can be found, e.g., in ref. 22, although this reference is for solid state materials. Recently Furuike *et al.*[23] studied axleless F_1-ATPase and found that neither fixed pivot nor rigid axle is needed for rotation of F_1-ATPase. Their observation seems to suggest that some physical factors are involved in the mechanism of F_1-ATPase rotary motor in addition to chemically specific factors.

Appendix 1. Flagellar rotary motor and F_oF_1-ATP synthase rotary motor

F_oF_1-ATP synthase is another example of biological rotary motors. Protons pass through the channels by the transmembrane electrochemical potential, which causes the rotor rotation. The diameter of F_oF_1-ATP synthase is about 10 nm[24], which consists of F_0c ring and γ protein. The γ protein molecule which rotates in F_1 has a diameter of about 2 nm, and has binding sites at every 120°. The γ protein molecule is

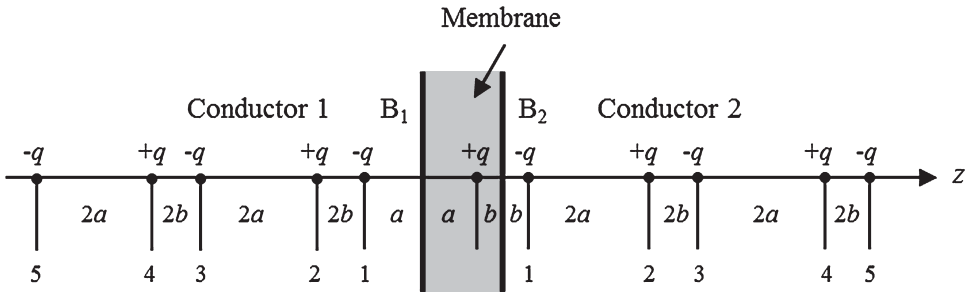

Figure 9 Distribution of the real and imaginary charges in the method of images to calculate E_x in Figure 2.

surrounded by about 10 F_0c-subunits[25]. About 10 protons can cause 360° rotation of the rotor. This means that one proton passage per F_0c-subunit is enough to cause one revolution of the rotor. Reversibility of the motor is possible: in-flow protons cause ATP synthesis and ATP hydrolysis causes the proton pumping (for instance, cf. ref. 25). Presumably each step of the proton motion is closely connected with each step of chemically specific reaction, as proposed e.g., in refs. 26, 27.

In the case of the flagellar rotary motor, the diameter of the flagellar motor is about 45 nm (cf. Figure 1 of ref. 4) compared to 10 nm of F_oF_1-ATP synthase[24]. The stator consists of about eight pairs of the Mot complex and about 1200 protons are needed for one revolution of the rotor[4]. Hence 1200/8 = 150 step movements of Mot* are needed per one revolution. It seems difficult to suppose 150 chemical reaction sites per a Mot complex. There is no observation of proton pumping for the bacterial flagellar motor.

These differences between the two rotary motors seem to suggest that the flagellar rotors are driven by a chemically non-specific force such as proposed in our model.

Appendix 2. Approximate electric field in Mot* produced by a proton in the channel

In Sect. 2.2, Figure 2 shows E_x to give an idea on the volume-averaged x component of the electric field in Mot*. The way to calculate E_x is outlined in this Appendix.

The calculation is based upon the method of images originated by Lord Kelvin. In many textbooks of electromagnetism, the method of images is explained by calculating the electric field in the case that an electric charge sits in uniform dielectric medium which occupies the space of $x > 0$ with a flat surface at $x = 0$ while a conductor exists infinitely in $x < 0$. The method of images can be used for the case that the uniform flat dielectric medium is sandwiched by two conductors as shown in Figure 9 (cf. refs. 28, 29). The blue area shows the membrane of the dielectric medium. The real electric charge is indicated by +q in the blue area. Imaginary electric charges +q and -q are set outside of the blue area on the line z which is perpendicular to the membrane. The imaginary charges are set so that the distribution of all charges is anti-symmetric referring to the two surfaces of the blue area. The electric field in the membrane can be calculated by the method of images with this charge distribution.

For numerical calculation, the position of the real charge (+q in the blue area) is denoted as z_p and the membrane thickness is denoted as d_{ch}, which is set as $d_{ch} = 7$ nm. The relative dielectric constant of the membrane ε is set as $\varepsilon = 2$. The electric field in the membrane is calculated as a function of z_p, which varies from 0 to d_{ch}. We are interested in the order of magnitude of volume-averaged x component of the electric field in Mot* which is denoted as E_x. The size of Mot* is unknown and is assumed to be equal to 2.5 nm (about the half of the diameter of MotA estimated on Figure 1 of ref. 4 drawn to scale). A cylinder of a radius 2.5 nm is considered in the membrane in Figure 9 with its axis on the z axis. The volume-averaged E_x is calculated for the half of the cylinder with positive x.

Appendix 3. On the piezoelectric activity of Mot*

At the end of Sect. 2.2, a question arises how large the piezoelectric activity of Mot* should be to realize the motor rotation. To answer the question, let us consider the system as drawn in Figure 10, where Mot* directly attaches to the rotor without the viscoelastic medium in Figure 1.

Since about 1200 proton passages[4] produce the rotor rotation of 2π, the rotor surface moves by $2\pi r_R/1200$ per one proton passage where r_R is the radius of the rotor. According to Figure 1 of ref. 4, r_R is about 12 nm, then the movement of the rotor surface, $2\pi r_R/1200$ is about 0.063 nm, and the problem becomes whether the piezoelectric deformation of Mot* can produce this step motion. The strain x_y corresponds to the change of the angle α in Figure 1(a) due to E_x. Here the length of Mot* along the x axis is set equal to 2.5 nm as in Appendix 2. Then the left edge of Mot* moves by $2.5x_y$ nm due to x_y when the right edge is fixed. If we set $2.5x_y$ nm = 0.063 nm, we get $x_y = 0.025$. Let us define d_M by $d_M = x_y/E_x$, then for $E_x = 10^8$ V/m (cf. Figure 2), d_M is given by

$$d_M = 2.5 \times 10^{-10}\ \text{m/V}. \tag{51}$$

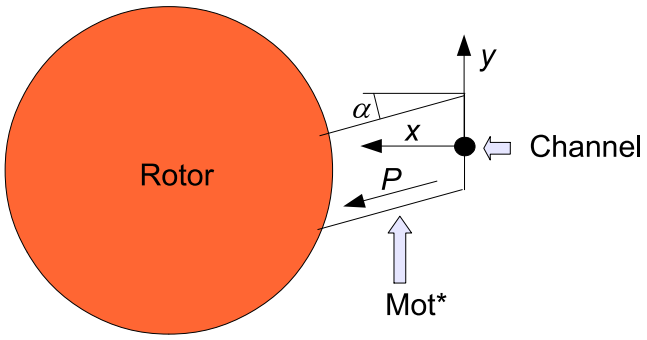

Figure 10 The case that Mot* contacts with the rotor, imagined to discuss piezoelectric activity of Mot*.

Mot* should have d_M of this order of magnitude to rotate the rotor.

Discussion on piezoelectricity for solid state materials is given, e. g, in ref. 30, and for ferroelectric materials in ref. 22. Presumably detailed investigation of piezoelectricity has not been done on polymers. In the linear approximation, discussion is done by using such equations as $x_i = s_{ij}X_j + d_{ij}E_j$ (Eq. 7.8a on p. 36 of ref. 22). Here x_i (i = 1, 2, 3, 4, 5, 6) is a component of strain tensor, X_j (j = 1, 2, 3, 4, 5, 6) is a component of stress tensor and E_j (j = 1, 2, 3) is a component of electric field. d_{ij} is called a piezoelectric strain constant. Usually experiments are done putting $X_j = 0$. Then $d_{ij} = x_i/E_j$ which is considered as a measure of piezoelectric activity. Experimentally observed values of d_{ij} distribute in the wide range depending upon materials. For example, $d_{11} = 2.3\times10^{-12}$ m/V in quartz[31] while d_{36} becomes as large as 2×10^{-8} m/V in KH_2PO_4 (Figure 33A-1-122 on p. 301 in ref. 32). In the case of the ceramic PZT which is commonly used for piezoelectric devices, d_{33} is about 3×10^{-10} m/V. (Figure 1C-a63-020 on p. 371 of ref. 33), which is comparable to the above value of d_M. Presumably d_{ij} can be larger in soft materials than solid materials. Judging from these experimental data, it seems possible that Mot* is designed as a shear stress transmitter to rotate the rotor.

References

1. Berg, H. C. *E. coli in Motion*. (Springer, Berlin, 2004).
2. Minamino, T., Imada, K. & Namba, K. Mechanism of type III protein export for bacterial flagellar assembly. *Mol. BioSyst*. **4**, 1105–1115 (2008).
3. Minamino, T., Moriya, N., Hirano, T., Hughes, K. T. & Namba, K. Interaction of FliK with the flagellar hook is required for efficient specificity switching. *Mol. Microbiol.* **74**, 239–251 (2009).
4. Berg, H. C. Constraints on models for the flagellar rotary motor. *Philos. Trans. R. Soc. Lond. B Biol. Sci.* **355**, 491–501 (2000).
5. Mitsui, T. & Ohshima, H. Shear stress transmission model for the flagellar rotary motor. *Int. J. Mol. Sci.* **9**, 1595–1620 (2008).
6. Braun, T. F. & Blair, D. F. Targeted disulfide cross-linking of the MotB protein of Escherichia coli: Evidense for two H^+ channels in stator complex. *Biochemistry*, **40**, 13051–13059 (2001).
7. Tanford, C. *Physical Chemistry of Macromolecules*. (John Wiley & Sons Inc., New York, 1961).
8. Oosawa, F. & Asakura, S. *Thermodynamics of the Polymerization of Proteins*. pp. 66–67 (Academic Press, New York, 1975).
9. Wakaki, M. (Ed.). *Physical Properties and Data of Optical Materials.* p. 315 (CRC Press, New York, 2007).
10. Ferry, J. D. *Viscoelastic Properties of Polymers*. (John Wiley & Sons, Inc., New York, 1960).
11. Saito, N. *The Physics of Polymers* (in Japanese), Chapter 7. (Shokabou, Tokyo, 1976).
12. Langevin, D. *Viscoelasticity of monolayers*. In *Encyclopedia of Surface and Colloid Science*. pp. 5584–5599 (Dekker, New York, 2002).
13. Fung, D. C. & Berg, H. C. Powering the flagellar motor of Escherichia coli with an external voltage source. *Nature* **375**, 809–812 (1995).
14. Sowa, Y., Hotta, H., Homma, M. & Ishijima, A. Torque-speed relationship of the Na^+-driven flagellar motor of *Vibrio alginolyticus. J. Mol. Biol*. **327**, 1043–1051 (2003).
15. Manson, M. D., Tedesco, P. M. & Berg, H. C. Energetics of flagellar rotation in bacteria. *J. Mol. Biol*. **138**, 541–561 (1980).
16. Berg, H. C., Manson, M. D. & Conley, M. P. Dynamics and energetics of flagellar rotation in bacteria. *Symp. Soc. Exp. Biol*. **35**, 1–31 (1982).
17. Berg, H. C. & Turner, L. Torque generated by the flagellar motor of Escherichia coli. *Biophys. J*. **65**, 2201–2216 (1993).
18. Berry, R. M. & Berg, H. C. Torque generated by the bacterial flagellar motor close to stall, *Biophys. J*. **71**, 3501–3510 (1996).
19. Berry, R. M. & Berg, H. C. Absence of a barrier to backwards rotation of the bacterial flagellar motor demonstrated with optical tweezers. *Proc. Natl. Acad. Sci. USA* **94**, 14433–14437 (1997).
20. Jones, C. J. & Aizawa, S. The bacterial flagellum and flagellar motor: Structure, assembly and function. *Adv. Microb. Phys.* **32**, 109–172 (1991).
21. Mitsui, T. & Ohshima, H. Theory of muscle contraction mechanism with cooperative interaction among crossbridges. *BIOPHYSICS* **8**, 27–39 (2012).
22. Mitsui, T., Tatsuzaki, I. & Nakamura, E. (translated from Japanese by Ishibashi, Y.; Tatsuzaki, I; Nakamura, E. & Burfoot, J. C.) *An Introduction to the Physics of Ferroelectrics.* (Gordon & Breach, New York, 1976).
23. Furuike, S., Hossain, M. D., Maki, Y., Adachi, K., Suzuki, T., Kohori, A., Itoh, H., Yoshida, M. & Kinoshita Jr., K. Axleless F_1-ATPase rotates in the correct direction. *Science* **319**, 955–958 (2008).
24. Abrahams, J. P., Leslie, A. G. W., Lutter, R. & Walker, J. E. Structure at 2.8 Å resolution of F_1-ATPase from bovine heart mitochondria. *Nature* **370**, 621–628 (1994).
25. Yoshida, M., Muneyuki, E. & Hisabori, T. ATP synthase—A marvelous rotary engine of the cell. *Nature Rev. Mol. Cell Biol.* **2**, 669–677 (2001).
26. Stock, D., Leslie, A. G. W. & Walker, J. E. Molecular architecture of the rotary motor in ATP synthase. *Science* **286**, 1700–1705 (1999).
27. Weber, J. & Senior, A. E. ATP synthesis driven by proton transport in F_1F_0-ATP synthase. *FEBS Lett*. **545**, 61–70 (2003).
28. Jackson, J. D. *Classical Electrodynamics.* (first edition) (John Wiley & Sons. Inc., New York, 1962).
29. Omoto, G. & Kogo, H. *Exercises on Electromagnetism*. (in Japanese) (Kyoritu. Tokyo, 1955).

30. Cady, W. G. *Piezoelectricity*. (Dover Publication, New York, 1964).
31. *IEEE Standard of Piezoelectricity*, ANSI/IEEE, Standard, p. 176 (New York, 1987).
32. Shiozaki, Y., Nakamura, E. & Mitsui, T. (Eds.). *Landolt-Börnstein Tables. Numerical Data and Functional Relationships in Science and Technology. Ferroelectrics and Related Substances*. Subvolume B1. *Inorganic Substances Other than Oxides.* (Springer, Berlin, 2004).
33. Shiozaki, Y., Nakamura, E. & Mitsui, T. (Eds.). *Landolt-Börnstein Tables. Numerical Data and Functional Relationships in Science and Technology. Ferroelectrics and Related Substances*. Subvolume A1. *Oxides: Perovskite-type oxides and LiMbO3 family*. (Springer, Berlin, 2001).